JOURNAL OF AIRCRAFT
Vol. 37, No. 6, November–December 2000

Exploratory Study of Aircraft Wake Vortex Filaments in a Water Tunnel

Kamran Rokhsaz,* Scott R. Foster,† and L. Scott Miller*
Wichita State University, Wichita, Kansas 67260-0044

The meandering nature of a single vortex filament is examined. The flowfield is typical of that in the vicinity of an aircraft wing tip vortex. Self-induced motion of the vortex filament is examined within the confines of potential flow theory and is compared with experimentally obtained results. A single-sensor constant temperature anemometer is used to measure the amplitude and rate of growth of vortex meandering experimentally. Data are presented that show the variation of the core radius with distance downstream of the point of origin as a function of the vortex strength. Also, experimental data are presented to show the variation in the amplitude of wandering downstream of the point of origin. Using the velocity fluctuations in the close proximity of a vortex filament, it is shown that 1) this quantity grows with downstream distance from the point of origin and 2) the degree of wandering depends on the vortex strength.

Nomenclature

C	= chord length
C_i	= amplitude
C_0, C_1, C_2	= curve-fitting constants
$d\boldsymbol{L}$	= increment of length along the vortex
$\boldsymbol{e}_x, \boldsymbol{e}_y, \boldsymbol{e}_z$	= unit vectors along x, y, and z
$f(x), g(x)$	= vortex spatial forms in x–y and x–z planes
I_z, I_y	= integrals given in Eq. (7)
L	= distance behind the $C/4$ point
$\boldsymbol{R}$	= vector of distance
r	= radial distance
r_c	= core radius
$\boldsymbol{r}_n, \boldsymbol{r}_m$	= radial vectors from mean vortex position
$T(t)$	= vortex temporal form
t	= time
U	= freestream velocity
u_n, v_n, w_n	= components of induced velocity
V_c	= composite velocity
$\boldsymbol{V}_n$	= vector of induced velocity
x, y, z	= coordinate axes
α	= damping in temporal motion
β	= frequency of temporal motion
Γ	= vortex strength
Γ_c	= composite vortex strength
γ_c	= nondimensional vortex strength, $\Gamma_c/(CU)$
λ	= nondimensional distance behind the $C/4$ point, L/C
σ	= standard deviation of the core position
τ	= nondimensional time, tU/C
χ	= reduced frequency, $C\beta/(2U)$

Introduction

BEHAVIOR of wing tip vortices has been the subject of intense research over the years. The bulk of the work in this area has been aimed at induced drag reduction by weakening or dispersing these vortices in the immediate vicinity of the aircraft or extraction of some of the energy contained within the intensely rotational flowfield. Some of these efforts are briefly outlined in Ref. 1. In some cases, although impractical, the proposed solution results in weakening of the wake turbulence. Examples include a wing tip turbine to extract some of the energy from the tip vortex[2,3] and placing splines in the wake to disperse the tip vortex.[4] More successful and practical applications include ogee tips,[5] winglets,[6] and wing tip sails.[7] However, in general, these methods have not been demonstrated to affect the structure of the trailing vortices in the far field that is hazardous to the following aircraft.

Aircraft wake vortex hazard has also been the subject of continuing research.[8,9] In prenatal methods, preventing the formation of strong and concentrated trailing vortices has been the primary goal. Different approaches have included manipulating the spanwise lift distribution and interfering with the rollup process. In postnatal methods, attempts have been made to disintegrate the already formed trailing vortices by destabilizing the vortex, inducing vortex breakdown, splitting the tip vortex into smaller vortices, and using methods to amplify the aging process. Comprehensive bibliographies pertaining to the aircraft wake vortex problem can be found in the literature.[10,11]

Reference 12 presents an extensive review of methods of longitudinal vortex control. According to Ref. 12, wing tip vortex stability can be altered by a variety of means, including suction or injection, interaction with other surfaces, ambient shear or stratification, or turbulence. Also according to Ref. 12, the instability excitation can be in the form of dynamic flowfield inputs to excite known instabilities.[13,14]

For many years, dynamic vortex instability was thought to be of the Crow instability type only.[15] This instability results from dynamic interaction of a single pair of vortex filaments and is due to mutual induction effects. This phenomenon has been observed in some atmospheric wake vortex degeneration events and in the laboratory.[16] Practical application of this phenomenon has been investigated by several sources. More recently, Crouch[17] explored the existence of other modes of dynamic instability resulting from mutual interaction of four vortex filaments. Such a vortex system is typical of that generated by aircraft in landing configuration with flaps extended. He showed the presence of two linear instability modes, much like that of Crow.[15] This result is expected because of the added degree of freedom. However, Crouch also explored the possibility of nonlinear effects leading to a third type of instability that he called "transient growth." The analytical results presented in Ref. 17 indicate the potential for wake vortex alleviation at rates several times higher than those of Crow instability.

It is critical to realize that any attempt at forced dynamic destabilization of a pair of vortex filaments must start with the thorough understanding of the nature and the behavior of such filaments. The potential flow model presented in Ref. 15 concerned the interaction

Received 22 February 2000; accepted for publication 17 June 2000.

*Associate Professor, Department of Aerospace Engineering. Associate Fellow AIAA.

†Graduate Research Assistant, Department of Aerospace Engineering. Student Member AIAA.

of a pair of wing tip vortices. However, as part of this model, the author examined the self-induced oscillation of a vortex filament. The conclusion drawn from this examination was that this effect results in a harmonic limit-cycle motion. However, as part of the analytical modeling, the spatial part of the solution was assumed to be harmonic a priori, and damping was allowed only in the temporal part of the solution.

Published results[18] represent a major step in such fundamental understanding of the flow behavior in the vicinity of a single vortex filament. Among the findings presented in Ref. 18 are the nature of meandering of a single vortex filament that is reported to be small in amplitude compared with the viscous core radius and a theory for correcting the measured velocities for the effect of this wandering. The core is reported to be laminar, and the vortex is said to be insensitive to the introduction of a probe. Therefore, velocity measurements can be made in the vicinity of the vortex with a constant temperature anemometer (CTA) probe. Furthermore, Davenport et al.[18] report that the wandering of the vortex core is random with about 95% of the kinetic energy lying below reduced frequency of unity.

The technical literature contains surprisingly little information, if any, about the characteristics of this meandering. Specifically absent is any information about the growth or the damping of the amplitude of this meandering, downstream of the point of origin. The present paper examines the meandering of a single vortex filament. The activities presented here are centered on measurements made in a water tunnel. Comparisons are made between the experimentally obtained data and the trends predicted by a potential flow model. The following items are discussed: 1) detailed data that show the variation of the core radius with distance downstream of the point of origin as a function of the vortex strength, 2) wandering frequency and amplitude as a function of vortex strength, and 3) variation of the wandering amplitude downstream of the point of origin.

Analytical Approach

Consider a single vortex filament in a stationary fluid, as shown in Fig. 1. The filament moves with the velocity that it induces on itself. Therefore, considering the motion of point n, one can write

$$\frac{\partial \boldsymbol{r}_n}{\partial t} + u_n \frac{\partial \boldsymbol{r}_n}{\partial x_n} = v_n \boldsymbol{e}_y + w_n \boldsymbol{e}_z \tag{1}$$

The second term on the left-hand side is of second order and is neglected in this analysis. The velocity components on the right-hand side can be determined from the Biot and Savart law that for an infinitely long vortex is stated as

$$\boldsymbol{V}_n = u_n \boldsymbol{e}_x + v_n \boldsymbol{e}_y + w_n \boldsymbol{e}_z = \frac{\Gamma}{4\pi} \int_{-\infty}^{+\infty} \frac{\boldsymbol{R} \times \mathrm{d}\boldsymbol{L}}{|\boldsymbol{R}|^3} \tag{2}$$

The goal here is to examine the velocity induced by a filament on itself, or self-induction. Therefore, we consider the effect of an element of length $\mathrm{d}L$ located at point m on point n along the same filament. Then

$$\boldsymbol{R}_{m,n} = (x_m - x_n)\boldsymbol{e}_x + (\boldsymbol{r}_m - \boldsymbol{r}_n) \tag{3}$$

where

$$(\boldsymbol{r}_m - \boldsymbol{r}_n) = [y_m(x_m, t) - y_n(x_m, t)]\boldsymbol{e}_y - [z_m(x_m, t) - z_n(x_m, t)]\boldsymbol{e}_z \tag{4}$$

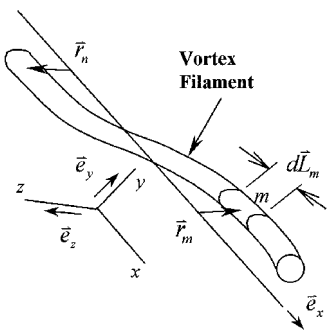

Fig. 1 Typical segment of a vortex filament.

$$\mathrm{d}\boldsymbol{L}_m = \left(\boldsymbol{e}_x + \frac{\partial y_m}{\partial x_m}\boldsymbol{e}_y + \frac{\partial z_m}{\partial x_m}\boldsymbol{e}_z\right)\mathrm{d}x_m \tag{5}$$

For separation of variables, the position of the filament relative to its mean location can be assumed to have the following form:

$$\boldsymbol{r}_m = T(t)[f(x)\boldsymbol{e}_y + g(x)\boldsymbol{e}_z] \tag{6}$$

Using this form in Eq. (3) and substituting the results in Eq. (2), one can arrive at the following expressions for v_n and w_n:

$$v_n = T(t)\int_{-\infty}^{+\infty} \frac{\Gamma}{4\pi|\boldsymbol{R}_{m,n}|^3}\left\{[g(x_m) - g(x_n)] - (x_m - x_n)\frac{\mathrm{d}g}{\mathrm{d}x}\right\}\mathrm{d}x_m$$

$$w_n = T(t)\int_{-\infty}^{+\infty} \frac{\Gamma}{4\pi|\boldsymbol{R}_{m,n}|^3}\left\{(x_m - x_n)\frac{\mathrm{d}f}{\mathrm{d}x} - [f(x_m) - f(x_n)]\right\}\mathrm{d}x_m$$

Substituting these expressions into Eq. (1) then results in

$$\boldsymbol{e}_y \int_{-\infty}^{+\infty} \frac{\Gamma}{4\pi|\boldsymbol{R}_{m,n}|^3}\left\{[g(x_m) - g(x_n)] - (x_m - x_n)\frac{\mathrm{d}g}{\mathrm{d}x}\right\}\mathrm{d}x_m$$
$$+ \boldsymbol{e}_z \int_{-\infty}^{+\infty} \frac{\Gamma}{4\pi|\boldsymbol{R}_{m,n}|^3}\left\{(x_m - x_n)\frac{\mathrm{d}f}{\mathrm{d}x} - [f(x_m) - f(x_n)]\right\}\mathrm{d}x_m$$
$$= [f(x_n)\boldsymbol{e}_y + g(x_n)\boldsymbol{e}_z]\frac{\mathrm{d}T/\mathrm{d}t}{T(t)} \tag{7}$$

Regardless of the form of $f(x)$ and $g(x)$, the integrals will have to be finite and can be denoted by I_z and I_y, respectively. Therefore,

$$\frac{\mathrm{d}T/\mathrm{d}t}{T(t)} f(x_n) = \frac{\Gamma}{4\pi} I_z \tag{8}$$

$$\frac{\mathrm{d}T/\mathrm{d}t}{T(t)} g(x_n) = -\frac{\Gamma}{4\pi} I_y \tag{9}$$

Both integrals must result in the same function $T(t)$. Therefore, the differential equation governing the temporal behavior of the vortex filament becomes

$$\frac{\mathrm{d}T}{\mathrm{d}t} = (\alpha + \beta i)T \tag{10}$$

where α and β are real constants and are given by

$$(\alpha + \beta i) = \frac{I_z \Gamma}{4\pi f(x_n)} = \frac{-I_y \Gamma}{4\pi g(x_n)} \tag{11}$$

Equation (11) can be thought of as a form of compatibility condition relating $f(x)$ and $g(x)$. It is clear that the motion of the filament in the fluid is governed by

$$T(t) = C_0 \exp[(\alpha + \beta i)t] \tag{12}$$

where C_1 is the constant of integration and depends on the initial condition.

It is obvious from Eq. (12) that the movements of a vortex filament remain bounded only if $\alpha \leq 0$. Experimental observations indicate that the amplitude of motion, while varying, remains bounded, implying that α can be negative. Furthermore, from Eq. (12), the degree of damping in the amplitude depends on the vortex strength. Study of this damping, negative or positive, was one of the goals of the current work.

The preceding analysis was performed for the case of a vortex filament in a stationary fluid. If the fluid moves at constant speed U, which is the case in a water tunnel, then t in Eq. (12) will be replaced by x/U.

Experimental Approach

Test Facility

Preliminary studies were performed in the water tunnel at the National Institute for Aviation Research (NIAR), located on the campus of Wichita State University (WSU). This facility is a closed-loop horizontal tunnel containing approximately 3500 gal of water. The clear test section is 2 ft wide, 3 ft high, and 6 ft long. A 2.5-ft segment with constant cross-sectional area connects the test section to the diffuser. This section can also be used as an extension of the test section, allowing observation of a vortex filament over a length of approximately 8 ft. The clear test section can be viewed from five different directions.

The tunnel is capable of reaching water speeds as high as 1 ft/s with very low levels of turbulence. The majority of the runs used for the current research were made at tunnel speeds of approximately 0.3 ft/s, corresponding to flow Reynolds numbers of 3×10^4/ft. The lowest level of freestream turbulence was visually observed at this speed, which also corresponded to the lowest tunnel vibration levels measured with an accelerometer. Flow visualization is primarily performed by dye injection, but hydrogen bubbles can also be used for this purpose. Figure 2 shows the schematic of this facility.

Test Apparatus

A sharp-edged rectangular blade, made from a 1/16-in.-thick flat plate, was used for vortex generation. The blade was mounted on a reflection plane away from the free surface at the top of the test section. Tip vortices were visualized through dye injection near the leading edge on the suction side of the blade. Figure 3 shows a dye stream visualizing a typical vortex filament that was obtained at angle of attack of 8 deg with tunnel speed of 0.31 ft/s, or chord Reynolds number of 2×10^4.

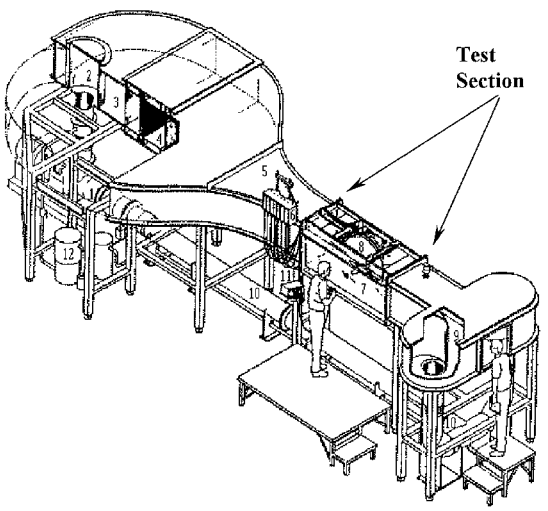

Fig. 2 Schematic view of the WSU/NIAR water tunnel.

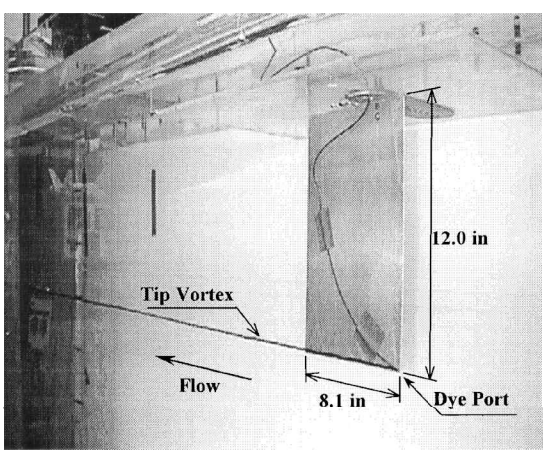

Fig. 3 Typical tip vortex used.

Flow Measurement

Quantitative data acquisition was performed using a single-channel CTA unit. The specific unit used for this research was a TSI Intelligent Flow Analyzer (IFA)-100. The single cylindrical sensing probe was attached to a two-axis, computer-controlled traverse system mounted on top of the tunnel. The system could be programmed to sweep a variety of planar regions or straight-line sections normal to the mainstream in either direction.

The tunnel speed was measured and calibrated against the pump speed control unit. Flow speed was measured by releasing dye in the water and measuring its time of travel between two marked locations that were 4 ft apart. These calibrations were repeated many times over the full range of tunnel speeds to ensure their repeatability and accuracy. Then, the CTA sensor was calibrated against the undisturbed freestream for two orientations, once with the sensor parallel to the freestream and once normal to the flow. Figure 4 shows example calibration curves, obtained in this manner, relating the IFA unit's voltage and the flow speed.

During measurements the CTA sensor was positioned parallel to the upstream flow and traversed very slowly upward and normal to the vortex filament, starting at the core. The sample rate used for data acquisition was set at 30–60 Hz. At each downstream position and for each blade angle of attack, at least 20 data sets were obtained. These velocity profiles were averaged to construct a model for the flow under those conditions. Figure 5 shows a typical composite velocity distribution obtained, following this procedure. The sensor normal orientation calibration data, or the top curve of Fig. 4, was utilized to obtain velocity values from the measured CTA output. The radial velocity components near the center of the core were assumed to be negligible.

As might be expected and as was observed early on, the single-sensor CTA readings were affected by both the vortex transverse and

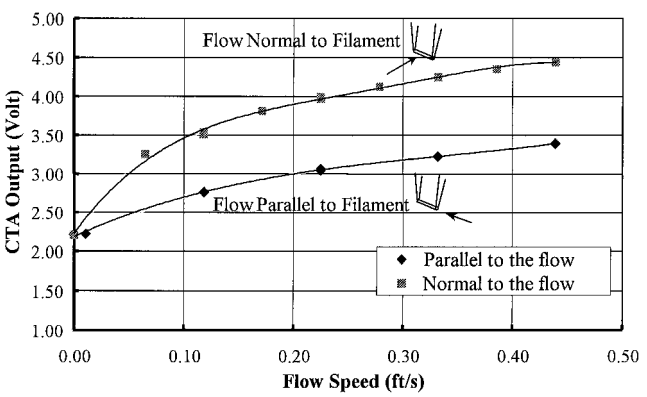

Fig. 4 Example calibration curves.

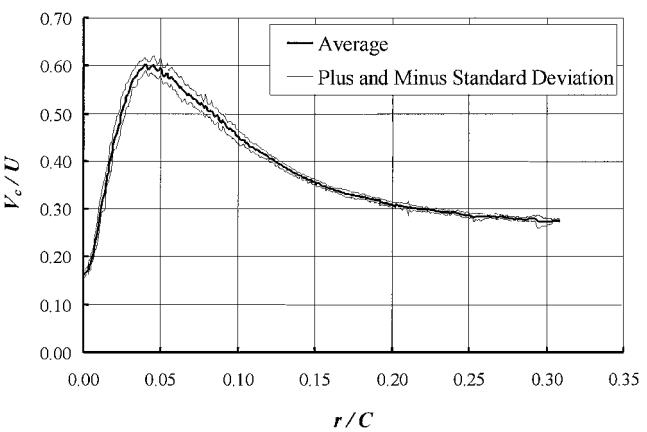

Fig. 5 Typical composite velocity distribution near the core.

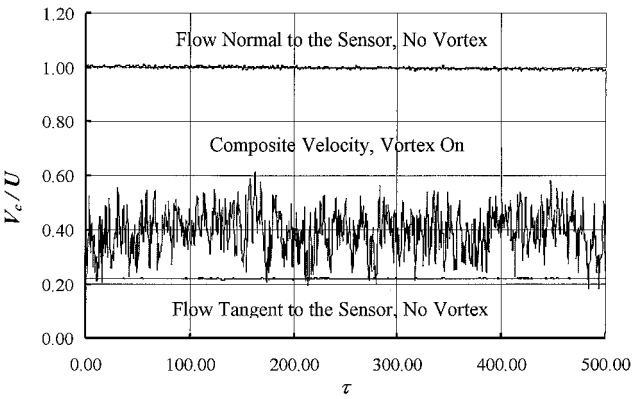

Fig. 6 Typical velocity fluctuations: angle of attack 10 deg, downstream distance 14 in.

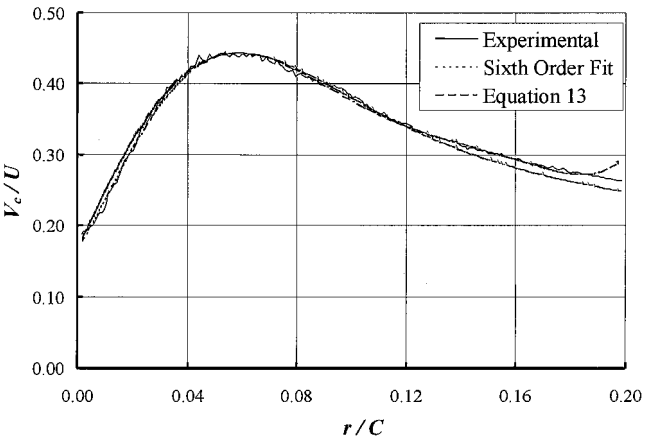

Fig. 7 Typical curve fit of the composite velocity.

axial velocity components. The latter component can be radically different from the freestream and can have a strong influence on the CTA signal. Furthermore, due to the required low CTA overheat ratio, dictated by the boiling point of water, the contributions of the two velocity components to the signal can be of the same order of magnitude. This effect is illustrated by looking at the results of the two calibrations shown in Fig. 4. The term composite velocity is used in this work to signify that both the axial and transverse velocity components are contributing to the CTA sensor output.

No attempt was made to separate the vortex velocity components for determining the meandering amplitude and frequency. Instead, the composite velocity distributions were simply fit using a sixth-order least-square method. The resulting functions thus relate average CTA sensor output to the distance from the core.

Characterizing the Wandering

To characterize vortex wandering, the CTA sensor was placed at a fixed distance very close to the filament center. Data were acquired at a rate of 200 Hz for a total of 30 min. Again, the CTA voltage signal was converted into composite velocity using the top calibration curve of Fig. 4. One such velocity history is shown in Fig. 6. Figure 6 also shows the velocity in the tunnel in the absence of the vortex. The top curve was obtained with the sensor normal to the freestream, whereas the bottom curve was acquired with the sensor parallel to the flow. These curves illustrate the relative magnitudes of velocity fluctuation with and without the vortex. The lowest frequency variations of these velocity data (which can be obtained via low-pass filtering) can be related to the vortex core distance and the wandering, by using the earlier developed sixth-order least-squared fit of average composite velocity distributions. Please note that the exact core coordinates cannot be determined using this method, only the scalar distances can be obtained.

Circulation and Core Radius

Because it was not possible to separate axial and transverse velocity component contributions to the CTA output, it was decided to model the composite velocity for quantifying the vortex circulation magnitude and core radius. Typical variations of the two velocity components are given in Ref. 18. These results clearly show the following:

1) Both velocity components, the transverse and the axial, vary in a nearly exponential manner, approaching a minimum near the vortex center.

2) The core radius associated with the axial velocity is almost twice as large as that of the transverse component.

Therefore, the following function was devised to curve fit the composite speed V_c sensed by the CTA:

$$V_c(r) = (\Gamma_c/2\pi r)\left\{\left[1 - \exp\left(-r^2/\, r_c^2\right)\right] + C_1 r\left[1 - \exp\left(-r^2/\, 2r_c^2\right)\right]\right\} + C_2 \qquad (13)$$

In this equation, Γ_c and r_c are representative of the circulation and core radius, respectively, whereas C_1 and C_2 were interpreted as constants for the curve fitting. It is reasoned that the first exponential term retains the characteristics of the transverse velocity component, whereas the other terms account for the axial velocity effect on the signal. The two velocity components cannot be separated using this function because the calibration curve used to obtain V_c is that corresponding to the case of flow normal to the sensor. However, the essential flow features in the vicinity of the core are retained in this manner.

Equation (13) contains four constants, Γ_c, r_c, C_1, and C_2, that had to be adjusted to curve fit the experimental data, subject to specific constraints. This fit was accomplished by forcing Eq. (13) to match the composite velocity distribution at the intercept, at the point of maximum velocity, and at a radius three times that of the point of maximum V_c. Furthermore, Eq. (13) was required to have zero slope at the point of maximum composite velocity. These conditions did not result in minimum error for the exponential fit. However, there was an excellent match between the composite velocity distribution and the resulting curve. Figure 7 shows a typical curve fit obtained in this manner for angle of attack of 8 deg and tunnel speed of 0.31 ft/s at 14 in. downstream of the blade.

Because the CTA output and, therefore, the velocity distribution were not symmetric about the vortex center, data from only one side were used for the purpose of this study. Such lack of symmetry is typical of vortex filaments emanating from a wing tip, as noted by other investigators.[16]

Results and Discussion

Data were obtained for a combination of three angles of attack at four locations downstream of the blade. The combination of the very low Reynolds numbers and the thin flat shape of the blade resulted in boundary-layer separation over most of the blade span, even at very small angles of attack. The separated boundary layers did not appear to interfere with the wake for angles of attack below 10 deg. However, at larger incidence angles, large-scale low-frequency eddies on the blade resulted in the time-dependent motion of the vortex filaments before their departure from the tip. Therefore, angle of attack was maintained below 10 deg. Downstream distances were measured relative to the one-quarter chord position along the blade. Normally, the distance behind a wing, required for complete wake rollup, is several times the wing span. However, in the present cases, the rollup process took place rather quickly because of the presence of separated boundary layers over a large part of the blade. This assertion is supported by the results presented in Fig. 8. It is quite evident from Fig. 8 that the circulation, as estimated from Eq. (13), does not change significantly downstream of the blade for the distances shown. Downstream distances varied between 14 and 50 in., in 12-in. increments.

The variation of the core radius, again estimated from Eq. (13), is shown in Fig. 9. It is clearly evident in Fig. 9 that r_c increases very slightly downstream of the blade. This behavior points to the fact that

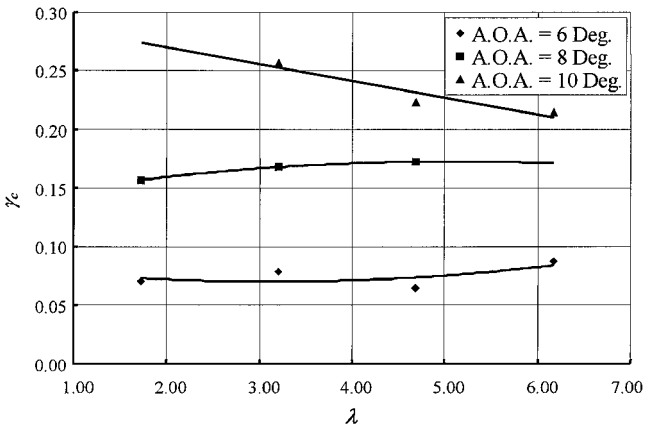

Fig. 8 Estimated circulation downstream of the blade.

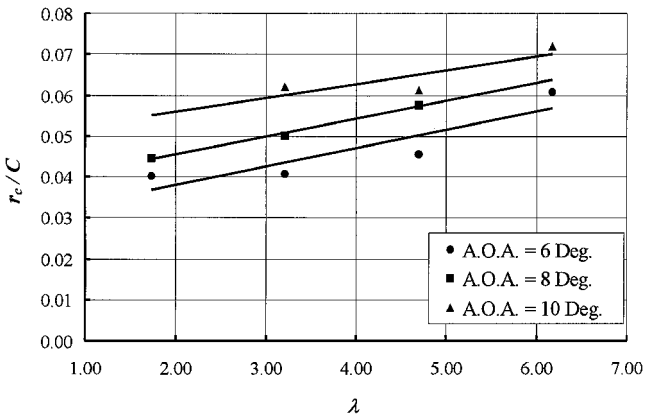

Fig. 9 Estimated core radius downstream of the blade.

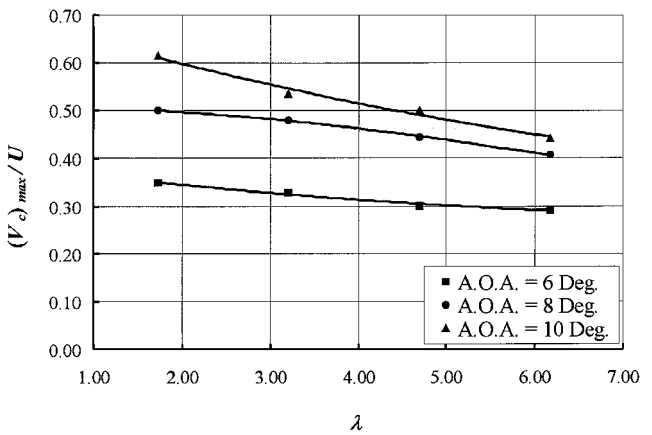

Fig. 10 Maximum composite velocity at several downstream distances.

the flow remains laminar and that turbulence plays an insignificant role in the time history of the CTA signal, which will be discussed later. The trends shown in Fig. 9 are also consistent with the exact analytical solution in two dimensions.[19]

Finally, the magnitude of the maximum composite velocity downstream of the blade is given in Fig. 10. Again, much like in Fig. 9, the monotonic decrease in this parameter and the relative variation in its magnitude are quite consistent with that predicted by Oseen and Hamel (see Ref. 19).

At each of the downstream locations and for each angle of attack, the vortex wandering was examined, according to the procedure outlined earlier. In every case, care was taken to ensure that the sensor remained very close to the center of the core, yet on only one side of the center. Furthermore, it was necessary for the sensor to remain

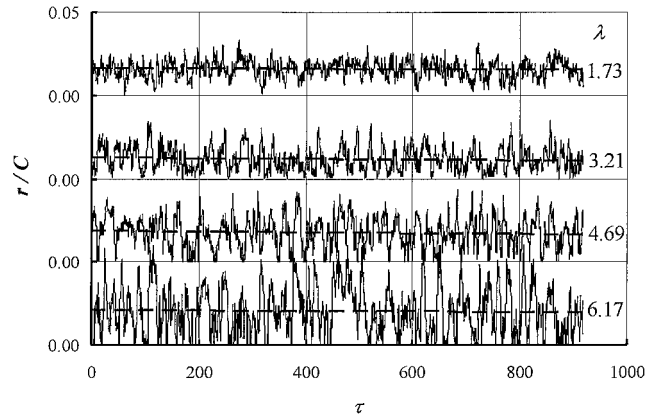

Fig. 11 Time history of the position of the core relative to the sensor for 6-deg angle of attack.

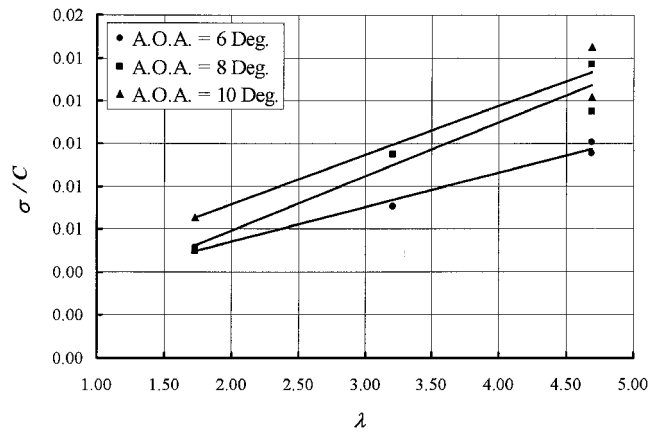

Fig. 12 Standard deviation of the vortex-core position relative to the sensor.

between the center of the core and the point of maximum composite velocity. As shown in Fig. 9, the latter point was approximately 0.5 in. from the center. Figure 11 shows the time history of the velocity fluctuations near the vortex for four downstream distances at angle of attack of 6 deg. The dashed lines in Fig. 11 correspond to the mean distance between the center of the core and the sensor. Similar data were obtained for the other two angles of attack and used to quantify vortex wandering. A careful examination of Fig. 11 shows some clipping of the data at 50 in. behind the blade. These points represent those cases where the composite velocity detected by the sensor was more that the peak value for that case (Figs. 7 and 10). This occurred only at 50 in. behind the blade and was due to the large amplitude of the filament motion. When the clipping became excessive, the integrity of the data was compromised, and therefore, those points were not used in the ensuing analysis.

Fourier transform of the data was obtained for each angle of attack and each downstream position. This analysis did not reveal any single dominant frequency, which supports the previously reported observations.[18] However, standard deviation of these data, which is related to the amplitude of wandering, showed a definite trend, as indicated in Fig. 12. A more detailed analysis is necessary to separate the actual magnitude of the meandering from the fluctuations due to turbulence. Nonetheless, the data shown in Fig. 12 support the statements made earlier, namely, 1) the growth rate of the wandering amplitude depends on the vortex strength and 2) for the cases considered here, the wandering amplitude grows with distance downstream from the point of origin. These results are consistent with those of the potential flow model that was presented earlier.

Again, as stated in the preceding paragraph, the reader is cautioned against attempting to relate these standard deviations to the amplitude of wandering directly. The manner in which these data were obtained renders such a direct relation impossible.

Conclusions

The self-induced motion of a single vortex filament was examined. A potential flow model was used to show that the amplitude of such motion could vary in time and describe the wandering motion of the filament. This model also indicated that the wandering amplitude would depend on the vortex strength.

Water-tunnel tests were performed to examine this phenomenon. A single-sensor CTA was used for data acquisition. A semi-analytical model was proposed for estimating circulation and core radius from the experimental data.

Using the velocity fluctuations in the close proximity of a vortex filament, it was shown that 1) the vortex motion is random and lacks any single dominant frequency, 2) the amplitude of motion grows with downstream distance from the point of origin, and 3) the degree of wandering depends on the vortex strength.

It is believed that a more detailed examination of the experimental results can yield clearer information about the nature and the amplitude of vortex meandering. Also, such information is necessary to complete the analytical model.

Acknowledgments

This work was partially supported by a National Science Foundation grant under the Experimental Program to Stimulate Competitive Research. The authors would like to recognize the invaluable assistance provided by Danny L. Ball, Ryan C. Laughton, and Renaud Rebours in carrying out this work.

References

[1]Rokhsaz, K., "A Brief Survey of Wing Tip Devices for Drag Reduction," *1993 SAE Transactions*, Vol. 102, Sec. 1, Society of Automotive Engineers, Warrendale, PA, 1994, pp. 1901–1910.

[2]Patterson, J. C., "Wingtip Vortex Turbine," U.S. Patent 4,917,332, April 1990.

[3]Patterson, J. C., and Fletchner, S. G., "Exploratory Wind-Tunnel Investigation of Wingtip-Mounted Vortex Turbine for Vortex Energy Recovery," NASA TN-2468, June 1985.

[4]Zalovcik, J. A., and Dunham, R. E., Jr., "Vortex Wake Research," *AGARD Symposium on Flight in Turbulence*, 1973, pp. 13.1–13.14.

[5]Vogel, J. M., "An Application of the Ogee Tip," *Proceedings of NASA–Industry–University–General Aviation Drag Reduction Workshop*, Univ. of Kansas, 1975, pp. 191–202; also NASA CR-145627.

[6]Whitcomb, R. T., "A Design Approach and Selected Wind Tunnel Results at High Subsonic Speeds for Wing-Tip Mounted Winglets," NASA TN-D-8260, 1976.

[7]Spillman, J. J., "Use of Wing Tip Sails to Reduce Vortex Drag," *Aeronautical Journal*, Vol. 82, No. 813, 1978, pp. 387–395.

[8]Rossow, V. J., "Prospects for Destructive Self-Induced Interactions in a Vortex Pair," *Journal of Aircraft*, Vol. 24, No. 7, 1987, pp. 433–440.

[9]Rossow, V. J., "Wake Hazard Alleviation Associated with Roll Oscillations of Wake-Generating Aircraft," *Journal of Aircraft*, Vol. 23, No. 6, 1986, pp. 484–491.

[10]Donaldson, C. duP., and Bilanin, A. J., "Vortex Wakes of Conventional Aircraft," AG-204, AGARD, May 1975.

[11]Hallock, J. N., "Aircraft Wake Vortices: An Annotated Bibliography (1923–1990)," Federal Aviation Administration, Dept. of Transportation, Research Document DOT/FAA/RD-90-30, Jan. 1991.

[12]Bushnell, D. M., "Longitudinal Vortex Control—Techniques and Applications," *Aeronautical Journal*, Vol. 96, No. 958, 1992, pp. 293–312.

[13]Bilanin, A. J., and Widnall, S. E., "Aircraft Wake Dissipation by Sinusoidal Instability and Vortex Breakdown," AIAA Paper 73-107, 1973.

[14]Rossow, V. J., "On the Wake Hazard Alleviation Associated with Roll Oscillations of Wake Generating Aircraft," AIAA Paper 85-1774, 1985.

[15]Crow, S. C., "Stability Theory for a Pair of Trailing Vortices," *AIAA Journal*, Vol. 8, No. 12, 1970, pp. 2172–2179.

[16]Eliason, B. G., Gartshere, I. S., and Parkinson, G. V., "Wind Tunnel Investigation of Crow Instability," *Journal of Aircraft*, Vol. 12, No. 12, 1975, pp. 985–988.

[17]Crouch, J. D., "Instability and Transient Growth for Two Trailing-Vortex Pairs," *Journal of Fluid Mechanics*, Vol. 350, 1997, pp. 311–330.

[18]Davenport, W. J., Rife, M. C., Liapis, S. I., and Follin, G. J., "The Structure and Development of a Wing-Tip Vortex," *Journal of Fluid Mechanics*, Vol. 312, 1996, pp. 67–106.

[19]Schlichting, H., *Boundary Layer Theory*, 6th ed., McGraw–Hill, New York, 1968, pp. 81, 82.